A semisynthetic peptide-metalloporphyrin responsive matrix for artificial photosynthesis

Sun, Z.

Chapter 4

Cryo-EM structure of the self-assembly of tCsmA and ZnPP

4.0 Abstract

The 7_2 helical structure of the self-assembled tCsmA-ZnPP complex is resolved at about 7 Å resolution by the cryo-EM technique. Each strand of the 2-start helix contains two tCsmA peptide strands running antiparallel. The threads of tCsmA have the monomers organized in a head to tail manner. They twist and form a hydrophobic core, to embed ZnPP tetramers coordinated to the imidazole groups of the histidine. The study of the structure at moderate resolution is helpful for understanding the mechanism of the self-assembly and the interactions between chromophores, and chromophore-peptide interactions. This provides a structural basis for the rational design of semisynthetic building blocks for artificial photosynthesis.

Zhongwu Sun, Stefan Huber, Ludovic Renault, Christoph A. Diebolder, Arjen Jakobi, Huub de Groot. Cryo-EM structure of the self-assembly of tCsmA and ZnPP, *To be submitted*

4.1 Introduction

As described in chapter 2, the truncated CsmA (tCsmA) and zinc protoporphyrin IX (ZnPP) chromophore are able to form 7_2 helical filaments in KPi buffer. The specific aim of this chapter is to provide structural information at moderate solution to understand the self-assembly and the interactions between chromophores. Structures of macromolecular assemblies have been determined by X-ray crystallography, NMR spectroscopy and single particle cryo-electron microscopy (cryo-EM).[1-3] Cryo-EM is the most suitable method for helical reconstruction of the tCsmA-ZnPP self-assembly. Cryo-EM is able to determine structures of assemblies with molecular weights larger than 150 kDa with very small sample amounts.[4] It does not require crystals and it is possible to work from paracrystalline materials.

To perform helical reconstruction in 3D, a single particle like analysis was applied to cryo-EM data collected from large helical filaments of tCsmA-ZnPP using the RELION empirical Bayesian approach.[5-9] Helical structures provide a view from all sides in every single image of a filament. Although in single-particle analysis all relative orientations of the particle projection images are necessary, the repeating, asymmetrical units of helical structures have fixed relative orientations. Therefore, helical symmetry and the orientation of the image of an entire filament can also reduce the experimental noise efficiently by averaging over a large number of asymmetrical units. To determine the precise symmetry during the 3D reconstruction process, the RELION software was used to obtain class averages, perform 3D reconstruction and determine the helical symmetry. Moreover, the additional point group symmetry that appears to be present in the tCsmA-ZnPP self-assembly, was also determined with RELION. However, although RELION has the tools for helix reconstruction with little external guidance, it can give rise to artifacts.[10] The helical symmetry was therefore validated with SPRING, which is an excellent single-particle procedure to determine precise helical symmetry in Fourier space.[11] As a helical reconstruction package for electron cryo-micrographs, it is based on a class-based helical reconstruction scheme to explore the helical symmetry by reconstructing the 3D structure from a large number of symmetry combinations using a single class average. According to the cross-correlation of the power spectra of the class average and projections of the

reconstructed 3D model, the accurate helical symmetry can be determined from a large number of possible symmetry combinations.[10]

Using this combination approach, we present here the cryo-EM structure at moderate resolution of the tCsmA in complex with ZnPP and the resulting helical structure of the self-assembly. The structure reveals the overall organization of tCsmA scaffolds, the interaction between ZnPP and tCsmA, and how tetramer formation affects the ZnPP and its dipole-dipole interactions.

4.2 Experimental section

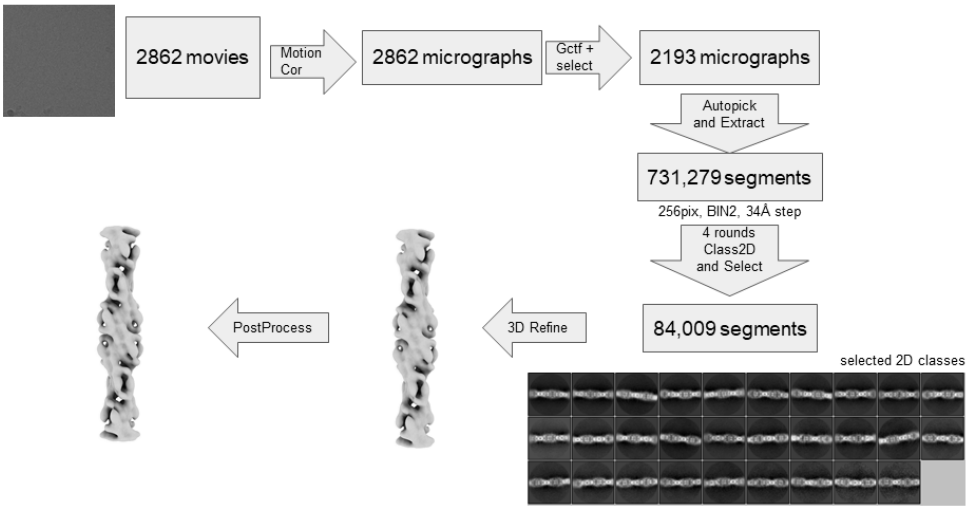

Figure 4.1 Processing scheme of cryo-EM data

Cryo-EM data were collected using a Titan Krios microscope at 300 kV. The experimental procedures are described in detail in Chapter 2. The data were transferred to a computer containing 4 NVIDIA GPU image processing units for pre-processing and helical symmetry determination with RELION 3.0. The helical symmetry determination with SPRING was performed with a CPU-based cluster. The final 3D reconstruction was performed in RELION 3.0. The processing scheme of cryo-EM data is shown in Figure 4.1. A total of 2193 micrographs were selected from 2862 raw movies. After 4 rounds of 2D classification, 84009 particles were selected for the 3D refinement. In addition, a cylinder mask with 6 nm diameter was applied during the initial 3D refinement. The helical rise was set to 34 Å in RELION. To make sure that a full helical unit is included in the analysis, this parameter should marginally

exceed the experimentally measured helical rise, which is about 32.9 Å. To fully observe the helix, a final box size of 256 Å was used to cover the 230 Å repeat for the 7_2 helical assembly. The details of the image processing are discussed in Results and Discussion.

4.3 Results and discussion

4.3.1 Cryo-EM images processing of the helical self-assembly

$$\text{Helical rise}_{1\text{-start}} = \text{rise}_{n\text{-start}}/n$$
$$\text{Helical twist}_{1\text{-start}} = (\text{twist}_{n\text{-start}} - 360°)/n \text{ for twist}_{n\text{-start}} < 0$$
$$\text{Helical twist}_{1\text{-start}} = (\text{twist}_{n\text{-start}} + 360°)/n \text{ for twist}_{n\text{-start}} > 0$$

Equation 4.1

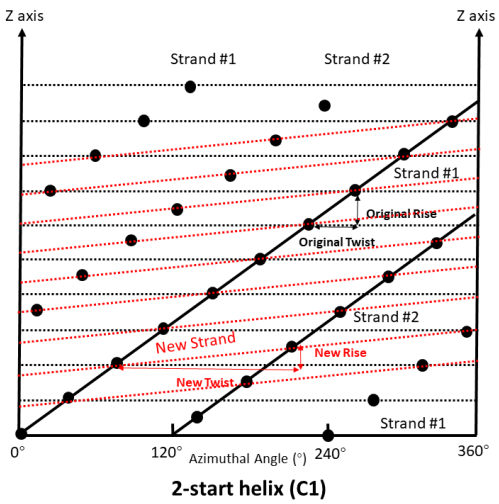

Figure 4.2 Two-start helix in a C1 point group symmetry representation, where instead of using the original twist and rise of the individual two strands (in black), RELION expresses the helical symmetry using a new twist and rise (in red).[10]

From the class averages the diameter of the filaments was determined as about 5 nm (Chapter 2, Figure 2.7B). The first step in resolving the structure was to apply a cylinder mask of 6 nm diameter to provide an initial electron density model, shown in Figure 4.3. In RELION only 1-start helices can be handled for 3D reconstruction. The procedure to convert the 2-start helix into a 1-start helix is schematically depicted in Figure 4.2. [10] This can be visualized by opening up the helix to form a 2D surface. n-start helices

always lead to a new helical twist and rise from the original twist and rise to represent the 1-start helix, where the new rise and twist are easily calculated using Equation 4.1.

The C1 point group symmetry analysis provides an unbiased (*i.e.* without a priori symmetry assumption) initial estimate of the helical reconstruction. In particular it indicates a 2-start helix (Figure 4.3).

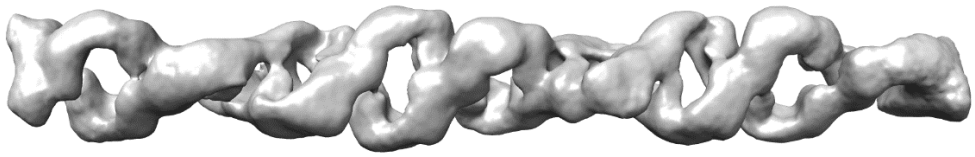

Figure 4.3 The initial electron density model without a priori symmetry assumption.

Except for helical symmetry, the self-assembly may also contain additional point group symmetry. The 2D class averages indicate rotational symmetry along the helix and perpendicular to the helix, pointing to D2 symmetry (SFigure 4.1). In addition, according to the optical data in Chapter 2, the tetrameric ZnPP clusters are highly symmetric with only one unique site, which indicates D2 point group symmetry (with three twofold axes through the tetrameric cluster) as well. For helices with D2 symmetry, the two separate strands of molecules are stacked against each other and all start from the same level along the Z axis. With point symmetry taken into account and validated, RELION can perform its empirical Bayesian single particle like analysis on the actual symmetry model, instead of the C1 reconstructed model according to Figure 4.2. To check the point symmetry guess, D2 symmetry without helical symmetry was applied for 3D reconstruction (Figure 4.4). Compared to the initial map (Figure 4.3), the 3D map with D2 symmetry shows more details (Figure 4.4B). In addition, the projection of the resulting map (Figure 4.4A) from D2 symmetry compares well with the 2D class average data (Figure 2.7B), with almost perfect overlap. This confirms that the helix contains additional D2 symmetry.

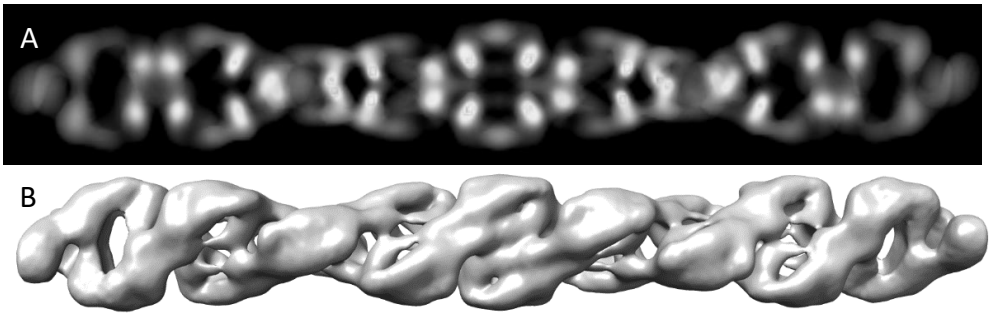

Figure 4.4 The projection image of resulting electron density map with D2 symmetry (A) and the corresponding electron density map (B).

To proceed with resolving the helical symmetry with D2 point symmetry, we determined from the 2D class averages initial estimates for the helical rise and twist (Figure 4.5). Here the initial guess is determined in Fourier space by taking the Fourier transform of a class average and determine the position of the layer lines. In Figure 4.5 a clear layer line at 1/32.9 Å is observed with intensity on the meridian, which serves as the initial guess for the helical rise in the reconstruction procedure. Since the image repeats itself after 113 Å, corresponding with a turn over 180°, a full turn corresponds to 226 Å, leading to 6.87 units in one helical turn with a 52.4° helical twist. This initial analysis is in line with the direct observations from the 2D class images in chapter 2.

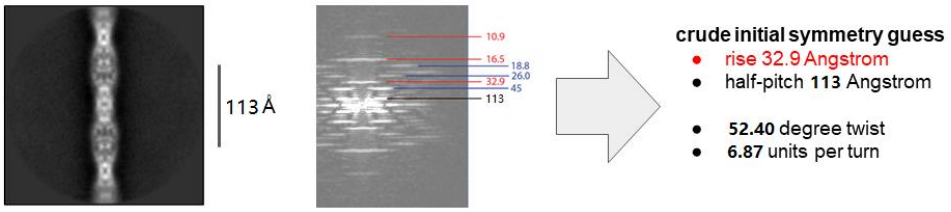

Figure 4.5 The crude initial helical symmetry guess based on the Fourier transform of a class average.

For refinement both D2 symmetry and helical symmetry with 52.4° for the helical twist and 32.9 Å for the helical rise were applied. However, comparing SFigure 4.1 to Figure 4.4B, the resolution is not improved after applying the helical symmetry. To validate the initial guess and get the precise helical symmetry, the helical parameters were confirmed using the SPRING helical analysis software (SFigure 4.2). The simulated power spectra fits the experimental data well. It confirms that the initial guess should be close to the real helical symmetry.

4.3.2 Cryo-EM structure of the helical self-assembly

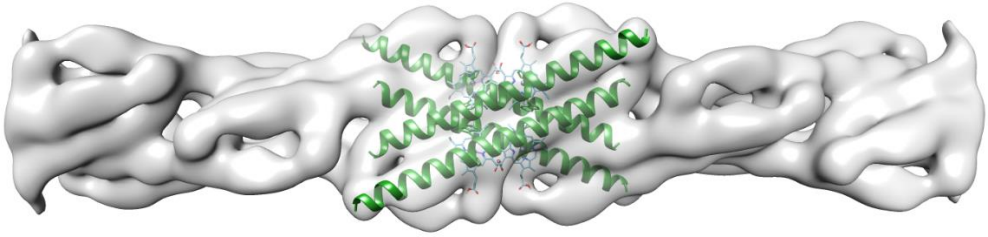

Figure 4.7 The electron density map fitted by the tetramer unit.

Under cryo-conditions, only single filaments stayed on the grid. They represent the same type of helical self-assembly which is helpful for the image processing. The 3D reconstruction map was obtained at about 7 Å resolution (Figure 4.7), which is sufficient to identify the helices and the ZnPP motifs. Interestingly, the homology model derived from the CsmA from the natural baseplate determined by NMR was found too long for matching to the electron density map. This can be attributed to the loop fragment from residue 30 to residue 35 in the homology structure (blue model in Figure 4.8). When this loop fragment is made helical, a fully extended rigid helix is obtained that is well in line with the EM structural data (Figure 4.7). Hence we propose there is no loop in the helix for the tCsmA-ZnPP complex. A fully helical tCsmA fragment is corroborated by the continuous electron density in the map, as a loop fragment should give rise to weaker electron density than for helical motifs. The straight alpha-helical tCsmA model simulated with the protein builder was used to fit the electron density map (Figure 4.7).[12] The stretched peptide helix model matches the NMR structure for residues 1-31 (red model in Figure 4.8) and fits well into the density map (Figure 4.7). Although a stretched helix derived from the structure proposed for the CsmA in the natural baseplate was also used to analyse the electron density (green model in Figure 4.8), this may be overstretched in the region of residues 1-31 and 35-43 as the peptide helix is too long and protrudes on both sides from the electron density map, giving a very poor fit. The filament helix is built from two parallel strands of tCsmA-ZnPP. Each strand is composed of antiparallel dimers of tCsmA-ZnPP with a P2 symmetry. Between the two strands, pairs of dimeric ZnPP are close to one another, and as a result, tetrameric units of ZnPP are formed. The complex forms a hydrophobic core, while the hydrophilic residues are

exposed to outside (Figure 4.10). This validates the interpretation of the optical data presented in Chapter 3.

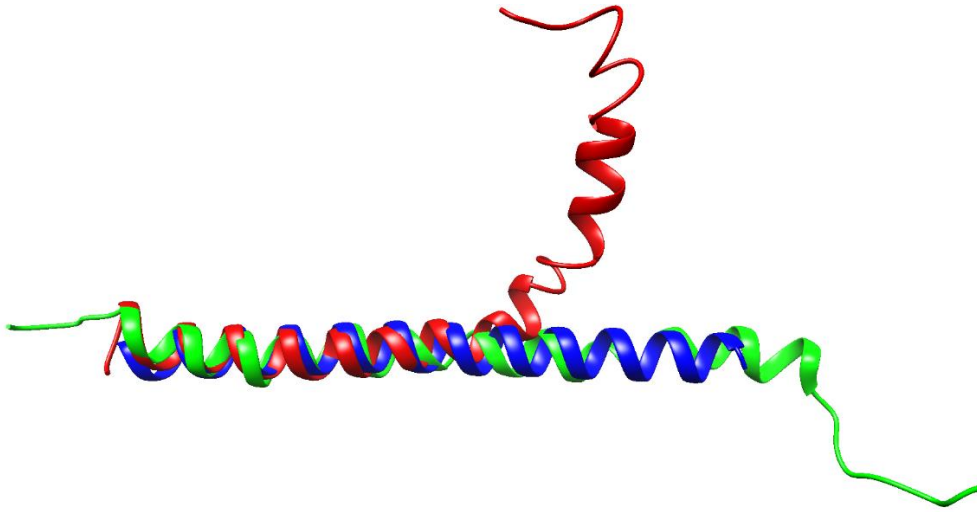

Figure 4.8 The simulated model of tCsmA (blue), the model from the natural baseplate (green) and the model of CsmA from NMR (red).

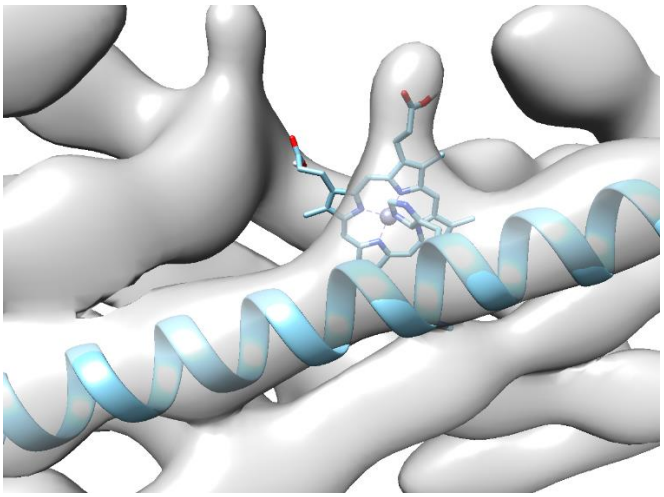

Figure 4.9 The possible fitting part of the propionic acid groups of ZnPP.

The electron density map is in line with coordination of the ZnPP at the H25 binding site (Figure 4.9). It also shows a small bump around the ZnPP, which can be attributed to one of the propionic acid groups -CH_2-CH_2-COOH (Figure 4.9). The rigid density indicates that the propionic acid group may interact with the peptide, for instance by forming a salt bridge, to make itself fixed. The dimeric unit in the tCsmA-ZnPP self-assembly shows some

similarity with the natural CsmA-BChl *a* complex.[13] The distance between the two ZnPP within an antiparallel tCsmA-ZnPP dimer is 21.1 Å, which is close to the distance between BChl *a* in the natural baseplate (Figure 4.10).[13] In addition, the two complexes cross with a similar angle as in the natural system. Having access to a model structure like tCsmA-ZnPP will be helpful to understand the mechanism of self-assembly and provide further refinement of the baseplate structure in the natural system.

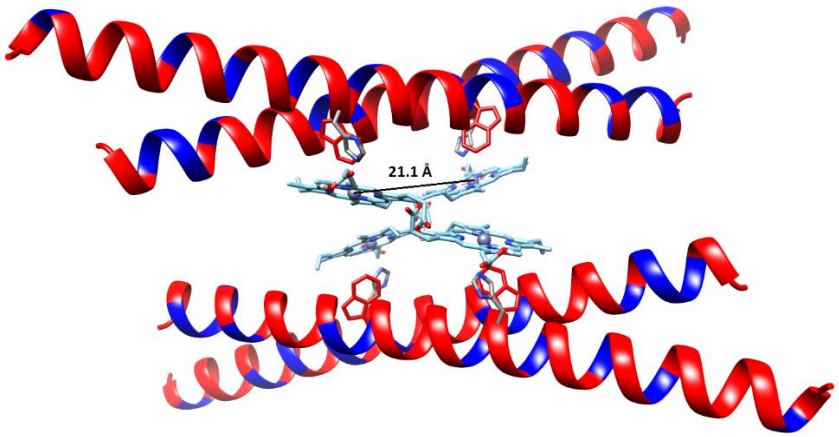

Figure 4.10 The tetrameric unit of the helical filament. The red colour presents hydrophobic parts and the blue colour is the hydrophilic part.

For the tCsmA-ZnPP complex in KPi buffer, each strand prefers to twist to stabilize a helical structure. As a result, the orientation of the complexes is nearly 90° rotated away from the orientation of the dimers in the planar arrangement observed in the natural system. On the one hand this allows to form a well-protected hydrophobic core with the ZnPP located inside, shielded from the environment by the outer peptide scaffold. In this arrangement, the salt bridges between peptide strands cannot contribute to stabilizing the self-assembly. In this way the structure indicates that the driving forces are mainly the hydrophobic effect and dipole-dipole interactions between the ZnPP. Since the charged residues are exposed towards the outside of the helix they can form salt bridges with other helixes to form bundles in KPi buffer when not on a grid (Chapter 3, Figure 3.4).

4.4 Conclusion

In conclusion, a refined 3D electron density map is obtained at a resolution of about 7 Å. The electron density map indicates a full alpha-helical structure and a fully helical simulated tCsmA-ZnPP model fits the map quite well. The complex forms a 7_2 helix in KPi buffer. Each strand is composed by dimeric tCsmA-ZnPP complexes which contain two antiparallel complexes with P2 symmetry. Dimeric ZnPP from the two strands are quite close to one another, and as a result, tetrameric units are formed.

4.5 References

1. Sali, A.; Glaeser, R.; Earnest, T.; Baumeister, W., *Nature* **2003,** *422* (6928), 216-225.
2. Jiang, W.; Ludtke, S. J., *Current Opinion in Structural Biology* **2005,** *15* (5), 571-577.
3. Chiu, W.; Baker, M. L.; Jiang, W.; Dougherty, M.; Schmid, M. F., *Structure* **2005,** *13* (3), 363-372.
4. Topf, M.; Lasker, K.; Webb, B.; Wolfson, H.; Chiu, W.; Sali, A., *Structure* **2008,** *16* (2), 295-307.
5. Scheres, S. H. W., *Journal of Molecular Biology* **2012,** *415* (2), 406-418.
6. Bricogne, G., *Acta Crystallographica Section A* **1984,** *40* (4), 410-445.
7. Murshudov, G. N.; Vagin, A. A.; Dodson, E. J., *Acta Crystallographica Section D* **1997,** *53* (3), 240-255.
8. Rieping, W.; Habeck, M.; Nilges, M., *Science* **2005,** *309* (5732), 303-306.
9. Frank, J., *Three-dimensional electron microscopy of macromolecular assemblies: visualization of biological molecules in their native state*. Oxford University Press: 2006.
10. He, S.; Scheres, S. H., *Journal of structural biology* **2017,** *198* (3), 163-176.
11. Desfosses, A.; Ciuffa, R.; Gutsche, I.; Sachse, C., *Journal of Structural Biology* **2014,** *185* (1), 15-26.
12. https://nova.disfarm.unimi.it/probuilder.htm.
13. Nielsen, J. T.; Kulminskaya, N. V.; Bjerring, M.; Linnanto, J. M.; Rätsep, M.; Pedersen, M. Ø.; Lambrev, P. H.; Dorogi, M.; Garab, G.; Thomsen, K., *Nature communications* **2016,** *7*, 12454.

4.6 Appendix

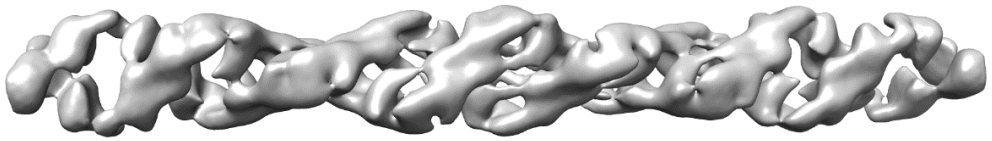

SFigure 4.1 The electron density map with D2 symmetry and helical symmetry (52.4° for the helical twist and 32.9 Å for the helical rise).

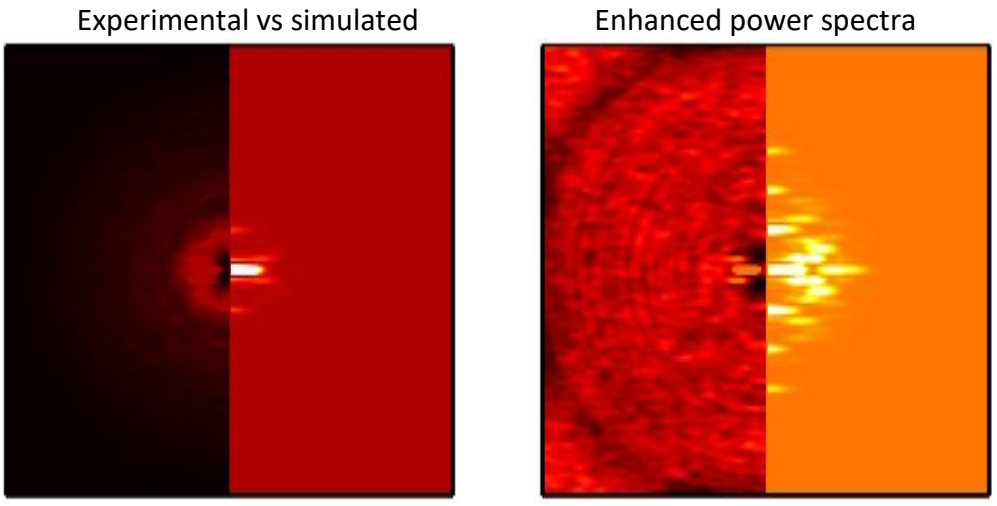

SFigure 4.2 The comparison chart of experimental and simulated power spectra based on the 2D class average images and the initial guess of the helical symmetry respectively (52.4° for the helical twist and 32.9 Å for the helical rise).